

# Nanocomposites



ISSN: (Print) (Online) Journal homepage: https://www.tandfonline.com/loi/ynan20

# Investigating the effect of surface modification on the dispersion process of polymer nanocomposites

Aditya Shanker Prasad, Yixing Wang, Xiaolin Li, Akshay Iyer, Wei Chen, L. Catherine Brinson & Linda S. Schadler

To cite this article: Aditya Shanker Prasad, Yixing Wang, Xiaolin Li, Akshay Iyer, Wei Chen, L. Catherine Brinson & Linda S. Schadler (2020) Investigating the effect of surface modification on the dispersion process of polymer nanocomposites, Nanocomposites, 6:3, 111-124, DOI: 10.1080/20550324.2020.1809250

To link to this article: https://doi.org/10.1080/20550324.2020.1809250

© 2020 The Author(s). Published by Informa UK Limited, trading as Taylor & Francis Group.	Published online: 28 Aug 2020.
Submit your article to this journal 🗹	Article views: 684
View related articles 🗹	View Crossmark data 🗹
Citing articles: 2 View citing articles	

# Tavlor & Francis Taylor & Francis Group

#### RESEARCH ARTICLE



# Investigating the effect of surface modification on the dispersion process of polymer nanocomposites

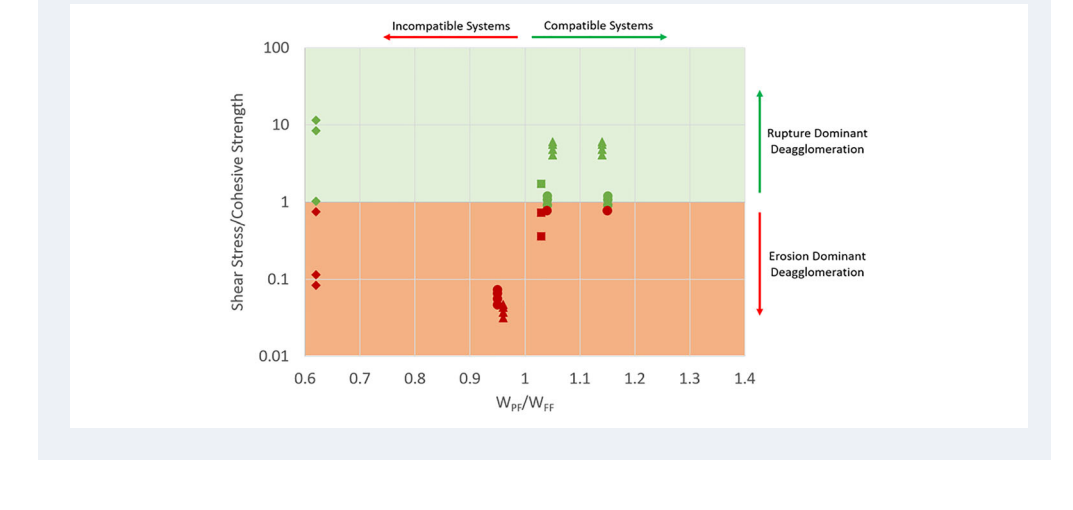
Aditya Shanker Prasad<sup>a</sup> , Yixing Wang<sup>b</sup>, Xiaolin Li<sup>b</sup>, Akshay Iyer<sup>b</sup>, Wei Chen<sup>b</sup>, L. Catherine Brinson<sup>c</sup> and Linda S. Schadler<sup>d</sup>

<sup>a</sup>Rensselaer Polytechnic Institute, Troy, NY, USA; <sup>b</sup>Northwestern University, Evanston, IL, USA; <sup>c</sup>Duke University, Durham, NC, USA; <sup>d</sup>University of Vermont, Burlington, VT, USA

#### **ABSTRACT**

Achieving controlled nanoparticle dispersion through melt processing has been challenging as processing-structure rules for polymer nanocomposites are still not well-defined. This work focuses on developing a quantitative understanding of the filler-matrix compatibility and melt mixing parameters on the dispersion of nanoparticles. Filler-matrix compatibility was varied by surface modification of silica nanoparticles. A twin screw extruder was used to prepare the nanocomposites and TEM imaging and image analysis were used to quantitively characterize the microstructure. It was found that matrix-filler compatibility strongly affected the method of agglomerate breakdown and dispersion. Under similar conditions, compatible systems tended to disperse via rupture of agglomerates while incompatible systems were found to disperse via erosion. A map was created to predict the dispersion mechanism as a function of processing conditions and system compatibility and systems from this study and literature were found to be in good agreement with the map.

#### **GRAPHICAL ABSTRACT**



#### **ARTICLE HISTORY**

Received 25 January 2020 Accepted 7 August 2020

#### **KEYWORDS**

Polymer nanocomposites; nanoparticle dispersion: TEM imaging; image analysis; surface modification

# Introduction

Polymer nanocomposites have the potential to improve efficiency and resilience of materials used in applications ranging from high voltage cable insulation to LED encapsulants [1-5]. However, commercial acceptance is limited because of poor control over nanofiller dispersion using commercial melt processing equipment. It is well-known that dispersion can be controlled enthalpic compatibilization and kinetic trapping after mixing, but the high surface area of nanofillers makes implementation challenging [6,7]. This

article aims to improve the quantitative understanding of the relationship between enthalpic compatibility and the processing parameters to achieve good dispersion.

The mechanisms that control agglomerate size as a function of shear rate and shear stress are wellunderstood [8-10]. Initially, the polymer melt wets the surface of the fillers and infiltrates the agglomerate. Shear generated due to the extrusion process breaks the agglomerates apart via rupture and/or erosion [11-14]. The failure of an agglomerate through the bulk is characterized as rupture. Breakdown of agglomerates through rupture leads



# octyl dimethyl methoxy silane

# chloro propyl dimethyl methoxy silane

# amino propyl dimethyl methoxy silane

Figure 1. Monofunctional silane surface modifiers used to vary the compatibility of the nanoparticle with respect to the polymer matrix.

to similarly sized smaller agglomerates. Erosion is defined as surface removal of nanoparticles from the agglomerate. In contrast to rupture, erosion leads to a size distribution of small and large agglomerates. Rupture occurs when the hydrodynamic shear stress exceeds the cohesive strength of the agglomerate and results in rapid de-agglomeration. Erosion occurs when the hydrodynamic shear stress can only pull one particle at a time from the agglomerate and de-agglomeration is slow. After de-agglomeration, the nanoparticles are distributed throughout the polymer matrix. Although these steps have been listed sequentially, they occur simultaneously.

In this study, the processing parameters (extruder screw speed, mechanical energy input from the extruder) and filler/matrix compatibility are systematically altered to better understand quantitatively how to achieve good dispersion. The effect of the infiltration of the polymer matrix on the cohesivity of the nanoparticle agglomerates is also investigated and a mechanism for determining the dominant deagglomeration mechanism is proposed. The surface of the nanoparticles (and thus the propensity for matrix infiltration of the agglomerates) is tuned using silane coupling agents. A twin screw extruder is used to process the nanocomposites. TEM imaging and image analysis is used to quantify the microstructure using a recently developed method for extracting quantified microstructure descriptors

Table 1. Compatibility of different surface modifications.

Polymer	Particle Surface modification	$W_{\rm PF}/W_{\rm FF}$
PMMA	Octyl silane	1.14
	Chloro silane	1.05
	Amino silane	0.96
PS	Octyl silane	1.15
	Chloro silane	1.04
	Amino silane	0.95

from the nanocomposites. The analysis is first carried out for PMMA nanocomposites with surface modified silica nanoparticles and then extended to PS nanocomposites, with the same nanoparticles and surface chemistries.

#### Materials and methods

Spherical nanoparticles of colloidal 14 nm silica dispersed in methyl ethyl ketone were procured from Nissan Inc. The matrices were polystyrene (PS) powder from Goodfellow Corporation and poly (methyl methacrylate) (PMMA) powder from Scientific Polymer Products Inc. As the polymer powders used were polydisperse in nature, this study did not look into the role of the molecular weight of the polymer matrix. Three monofunctional siloxanes (shown in Figure 1) were purchased from Geleste Inc. and used as received for particle modification. These were aminopropyledimethylethoxysilane (APDMES), chloropropyledimethylethoxysilane (CPDMES) and octyldimethylmethoxysilane (ODMMS) chosen for their varying compatibility with the matrix polymer. The compatibility was quantified by the metric of the ratio of the work of adhesion between the polymer-filler and the work of the adhesion between the filler-filler [4] (Table 1), where the filler represents the modified filler. Natarajan et al. [4] have determined these compatibility metrics using the Owens-Wendt model for estimating surface energies. Previous work using solvent mixing has shown that this ratio accurately predicts the tendency of a nanocomposite system to disperse or agglomerate [4]. When this ratio is less than one, the system is incompatible and the resultant nanocomposite has large agglomerates. When the ratio is greater than or equal to one, the individual nanoparticles are dispersed. The ratio of the work of adhesion also indicates the wetting behavior between polymer matrix and nanoparticle. It can also be considered as a ratio of the affinities of the polymer to filler and filler to filler.

Nanoparticle surface modification was carried out using the method elucidated by Natarajan et al. [4] 0.5 ml of monofunctional siloxane was mixed with 50 ml of tetrahydrofuran (THF) and 16 ml of silica nanoparticles in MEK solution and refluxed at 70 °C under a nitrogen atmosphere for 24 h. The solution was poured into 500 ml of hexane, kept in an ice

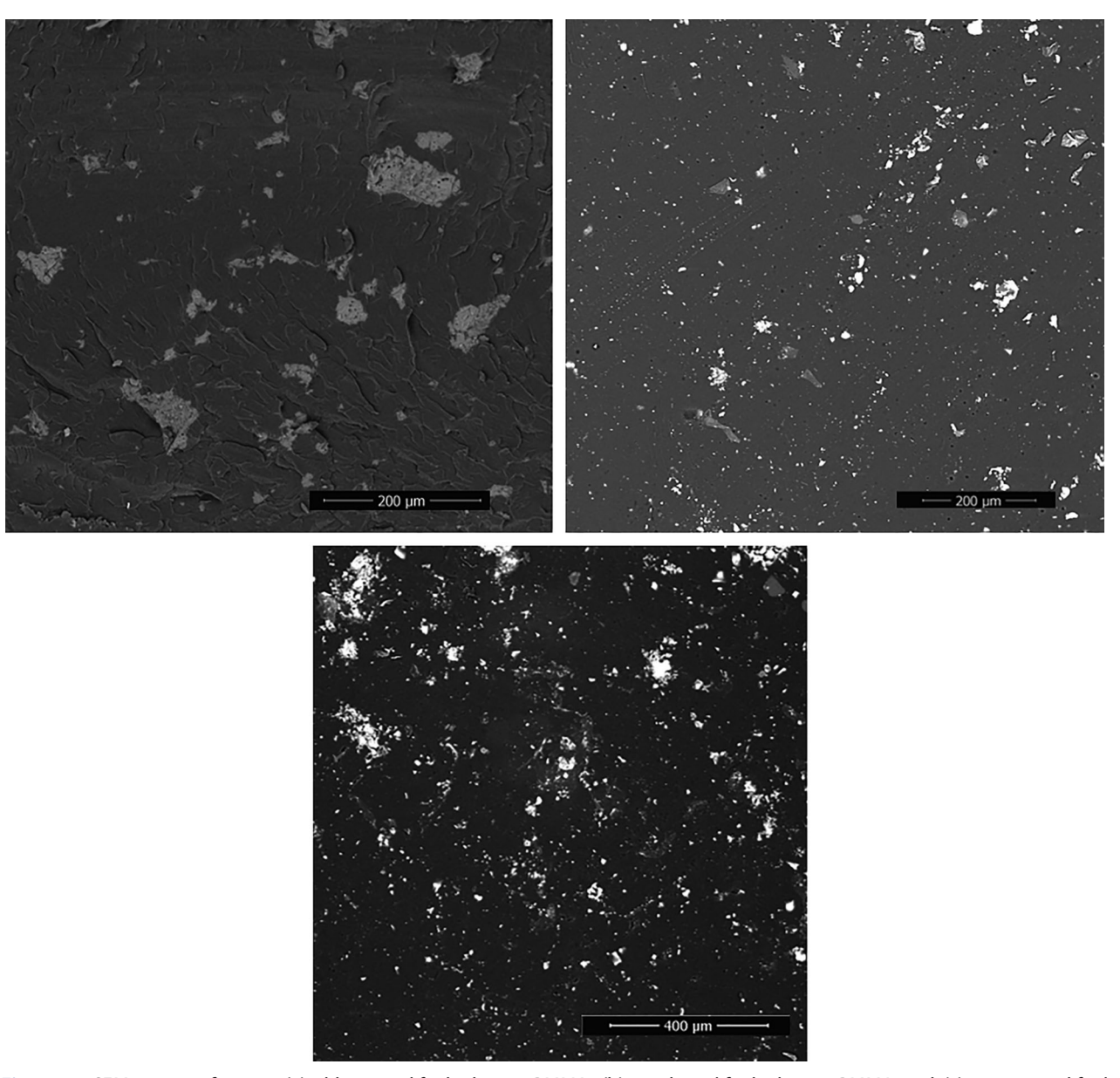


Figure 2. SEM image of 2 wt% (a) chloro-modified silica in PMMA, (b) octyl-modified silica in PMMA and (c) amino-modified silica in PS. The microstructure is filled with large agglomerates as the sample has only been hot pressed and not be subjected to extrusion processing.

bath, leading to precipitation of the nanoparticles. resulting mixture was centrifuged 10,000 rpm, 10 °C for 10 min. The supernatant was discarded, and the precipitate was re-dispersed in THF and the washing was repeated three times. The modified particles were re-dispersed in THF. Surface coverage of ~1 chain/nm<sup>2</sup> as determined from thermogravmetric analysis (TGA) was achieved. A small amount of DI water was added to the nanoparticle solution, leading to the precipitation of the nanoparticles. About 50% of the solvent was removed by heating the solution at 70 °C, following which, a small amount of polymer powder was added. The remaining solvent was removed in a roto-evaporator. The resulting polymer-particle powder was dried in a vacuum oven at 70 °C for 12 h and tested for the particle loading using TGA. Extra polymer powder was added to achieve a 2 wt% particle

loading and the mixture was passed through a jet mill to reduce the size of large macro agglomerates.

An FEI Versa 3D Dual Beam Focused Ion Beam/ Scanning Electron Microscopy (SEM) was used to characterize the prepared nanocomposite before extrusion and mixing. Nanocomposite powder was hot-pressed into rectangular shaped samples and fractured to expose the cross section. The exposed face was sputter coated to reduce the build-up of charge. To limit damage to the sample, the SEM was operated at 10 kV accelerating voltage and a back scatter detector was used to achieve contrast between the nanoparticle agglomerates and the matrix.

A Thermo Haake Minilab twin screw extruder was used to compound the composites. This extruder has a backflow channel for recycling of the polymer independent melt, allowing for

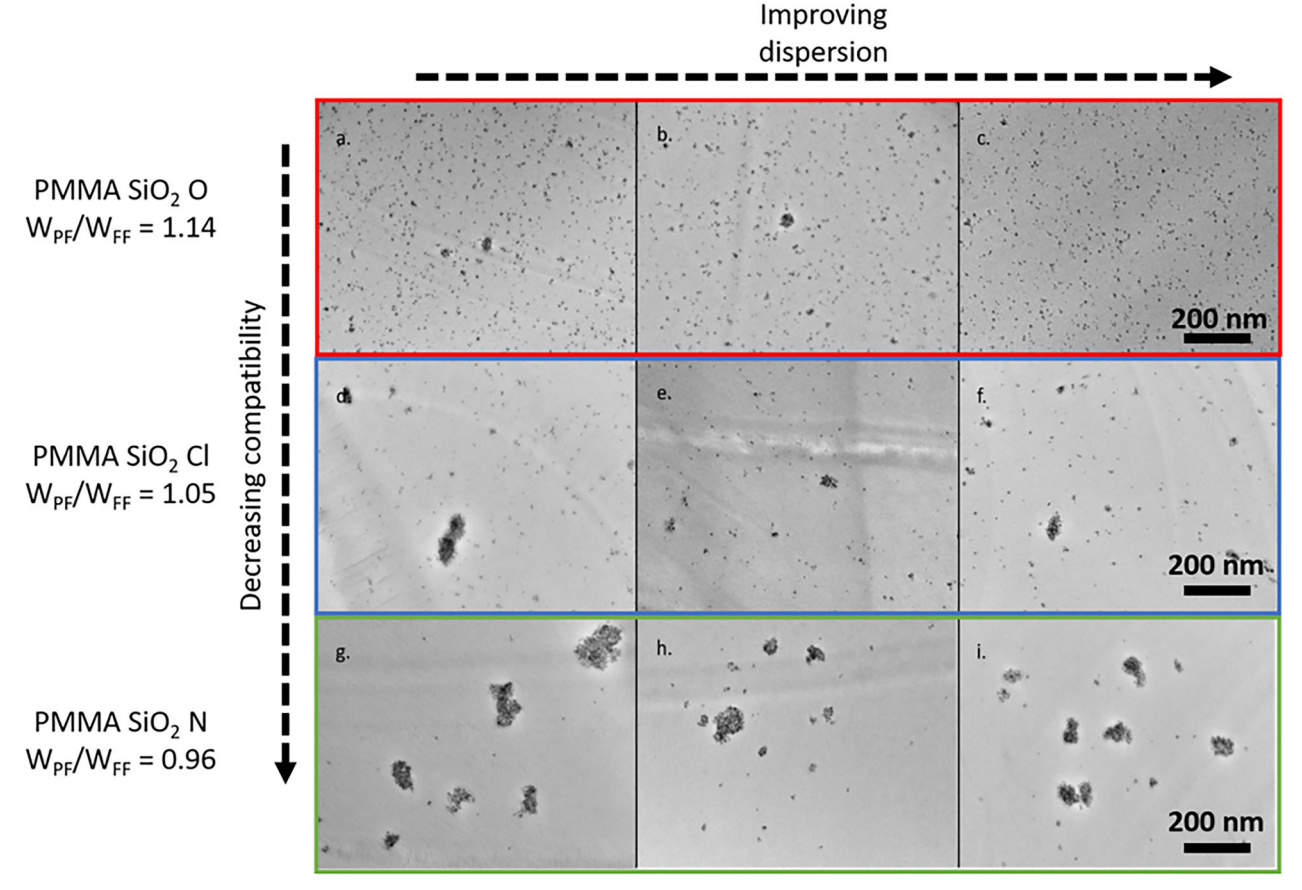


Figure 3. TEM images showing dispersions state for different PMMA-nanocomposite systems with filler loading of 2 wt%: (a-c) PMMA SiO<sub>2</sub> O; (d-f) PMMA SiO<sub>2</sub> Cl; (g-i) PMMA SiO<sub>2</sub> N. All scale bars are 200 nm.

manipulation of the residence time and screw speed. PMMA based composites were prepared at a temperature of 180 °C and PS based composites were prepared at 150 °C. The extruder was operated at different screw speeds (50,10,02,00,300 rpm). The specific mixing energy [15-17] for a mass m of sample was calculated using the torque  $(\tau)$ , screw speed (N) and time spent (t) in the extruder using Equation (1). Nanocomposites were created with different levels of energy input between 100 and 4000 kJ/kg by varying the residence time of the melt in the extruder.

Energy Input = 
$$\frac{\tau \times N \times t}{m}$$
 (1)

Using the aforementioned screw speeds, samples were created at with specific mixing energies ranging between 100 and 12,000 kJ/kg by varying the residence times between 10 s and 33 min.

Extruded samples were embedded in epoxy for ultramicrotomy using a diamond knife. Sections of 50 nm thickness were cut from the sample and deposited on a copper grid for microstructure examination under a TEM. A JOEL 2010 transmission electron microscope was operated at 200 kV and 30 images were taken for each sample to assess the dispersion state of the nanoparticles.

For extracting quantitative microstructure information, gray scale TEM images were binarized. A Niblack algorithm [18] was employed for the binarization, which uses a local thresholding technique to accurately identify polymer and particles. Binarized images were analyzed for key microstructural descriptors such as interfacial area ( $I_{\text{filler}}$ ), average cluster size and distribution of cluster sizes.  $I_{\rm filler}$ was calculated by taking the ratio of the number of pixels that make up the boundary of the nanoparticle cluster and polymer interface to the total number of filler pixels in the image. Higher values of I<sub>filler</sub> signify greater amounts of nanoparticle-polymer interface.

# **Results**

In this section, the results from the image characterization and analysis of the nanocomposite systems are presented. PMMA based nanocomposites results are presented first, followed by the results of PS based nanocomposites and a discussion on the model used to explain these results.

# Pre-extrusion microstructure

Figure 2 shows SEM images of hot pressed samples of PMMA SiO<sub>2</sub> Cl, PMMA SiO<sub>2</sub> O and PS SiO<sub>2</sub> N.

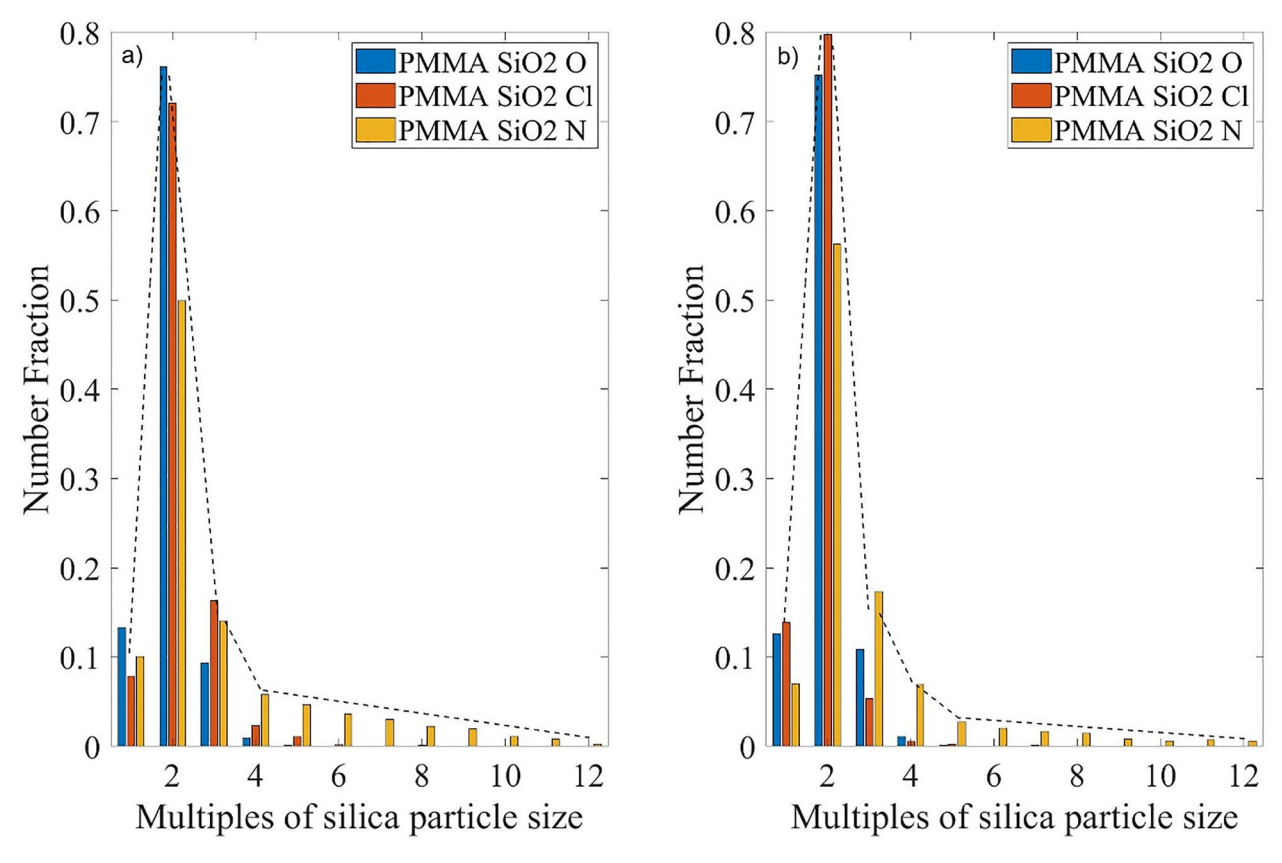


Figure 4. Nanoparticle size distributions at (a) 100 rpm and 200 kJ/kg processing energy and (b) 300 rpm and 4000 kJ/kg processing energy for different PMMA composites. All samples are at 2 wt% filler loading and have similar processing conditions.

These samples were created using the unmixed polymer nanocomposite power mixtures and represents the state of the nanocomposite before extrusion mixing. As these are pre-extrusion, the microstructures are characterized by agglomerates as large as several hundred microns across.

# PMMA nanocomposites post extrusion microstructure characterization

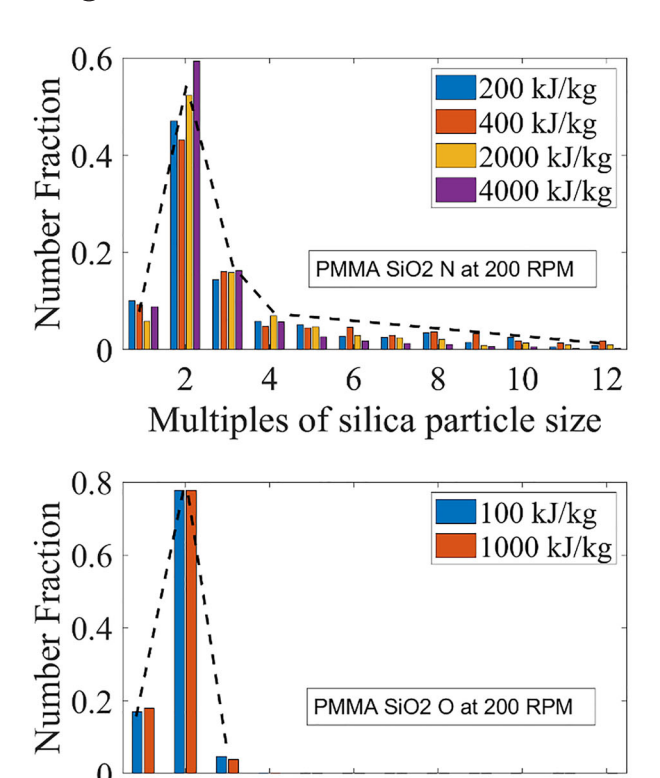
Figure 3 shows the TEM images obtained for the PMMA systems after the nanocomposite powder was processed through the extruder. The images presented are representative of the dispersion state for the different surface modifications. Qualitatively, the TEM images show that for the octyl modified silica, the nanoparticles are well-dispersed with few clusters. In contrast, the chloro and amino modified silica exhibit more clustering. The chlorosilane modified silica is characterized by few singly dispersed nanoparticles and many small clusters. The amino modified silica shows some large agglomerates and very few singly dispersed particles and many small clusters. Hence, there is a stark difference in the microstructure and dispersion state of the nanoparticles depending on their surface modification.

The distribution of the nanoparticle cluster sizes from 30 images is shown in Figure 4. The bin size for the plot is in multiples of the 14 nm particle

diameter. Figure 4a shows the distribution of nanoparticle clusters for PMMA systems at low screw speed (100 rpm) and low energy input (200 kJ/kg for amino and chlorosilane silica sample and 100 kJ/kg for the octylsilane silica sample). Figure 4b shows the distribution at high screw speed (300 rpm) and high energy input (4000 kJ/kg). At the lower processing energy and low screw speed (Figure 4a), the distribution depends strongly on compatibility. For octyl modified silica (compatible), ~98% of nanoparticle clusters are 0-42 nm (1 to 3 base silica particle diameters) and the distribution is narrow. For the chloro modified (compatible)  $\sim$ 95% are in the size range of 0-42 nm. For the amino modified sample (much less compatible), only ~73% of nanoparticle clusters are within  $3\times$  of the base particle diameter there is a long tail in the distribution in Figure 4a.

By increasing the screw speed and the energy input from the extruder (Figure 4b), the distribution for the octyl modified system remains narrow with  $\sim$ 99% of clusters in the first three bins of the histogram. Additionally, the distribution for the chloro modified system also becomes narrow with ~99% of clusters in the initial three bins. In contrast, only  $\sim$ 80% of the clusters are 0-42 nm for the amino modified silica. While this is an improvement over the low processing energy sample, a significant portion of large clusters remain.

2



6

Multiples of silica particle size

8

10

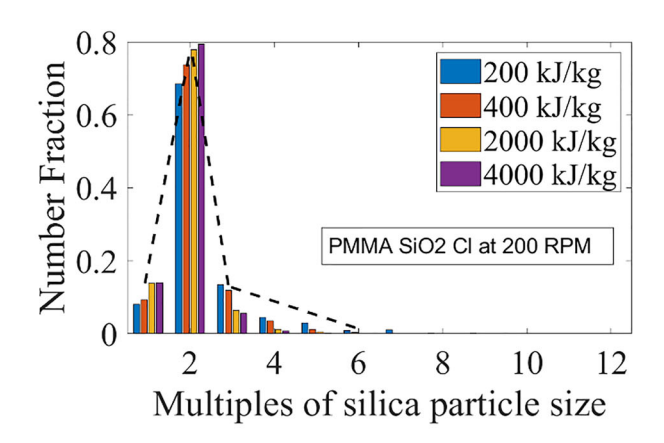


Figure 5. Nanoparticle cluster distribution for (a) amino modified silica samples, (b) chloro-modified silica samples and (c) octyl-modified silica samples. All samples have 2 wt% filler loading and have been processed at 200 rpm screw speed.

12

The quantitative assessment of the microstructure also allows for investigation of the development of the microstructure at the same screw speed. The evolution of the microstructure at 200 rpm screw speed and different energy inputs is shown in Figure 5. The energy input is varied by changing the processing time of the nanocomposite in the extruder (Equation (1)). For the amino modified system (incompatible), all samples show a broad distribution of nanoparticle clusters. With increasing energy input from the twin screw extruder, the number fraction of agglomerates between 1 and 2× silica diameters significantly increases. This is seen to be at the expense of larger agglomerates. However, these large agglomerates are not completely broken down and the tail of the histogram persists even at higher energy inputs, suggesting that the process of formation of small clusters from the large agglomerates is slow, typical of erosion. In comparison, for the chlorosilane modified silica system (compatible), there is a narrow distribution of agglomerate sizes that becomes narrower with increased energy input. Similar to the amino modified system, the increase in small clusters is at the expense of the larger agglomerates. The fraction of clusters up to 2× nanoparticle diameter (28 nm) in size increases from 0.76 to 0.93 while the fraction of clusters between 4 and 5 times the nanoparticle diameter decreases from 7% to less than 1%. Hence,

these large agglomerates are broken down at a faster rate, suggesting that the process of agglomerate size reduction is typical of rupture. The octyl modified silica system (compatible) (Figure 5c) shows a very narrow distribution of nanoparticle agglomerates even at very low processing energy, suggesting that the size reduction of agglomerates also occurred *via* rupture. Increasing the energy input by a factor of 10 does not affect the dispersion state.

To further quantify the results, we monitored interfacial area normalized by volume fraction ( $I_{\text{filler}}$ ) and average cluster radius as a function of mixing energy as calculated using Equation (1).

Figure 6 shows the evolution of  $I_{\text{filler}}$  at different screw speeds for the PMMA SiO<sub>2</sub> N, PMMA SiO<sub>2</sub> O and PMMA SiO<sub>2</sub> Cl samples. The range of values of  $I_{\text{filler}}$  depend on the surface modification. For the amino modified silica  $I_{\text{filler}}$  is between 0.06 and 0.09, while for the chloro modified silica and octyl modified silica,  $I_{\text{filler}}$  is between 0.15 and 0.24 and between 0.15 and 0.23, respectively. Over the processing energy range investigated, the PMMA SiO<sub>2</sub> N samples show a slow rate of increase in  $I_{\text{filler}}$ . At all screw speeds, the  $I_{\rm filler}$  is essentially flat. This suggests that there is not adequate hydrodynamic force for effective breakdown of agglomerates. The agglomerate size reduction is slow and does not reduce below  $\sim$ 54 nm for all processing conditions. For the same processing conditions, the PMMA

 $SiO_2$  Cl samples show higher values of  $I_{filler}$  and lower values of average cluster radius. For all screw increases rapidly (Figure  $I_{\rm filler}$ Agglomerates are also broken down at a faster rate and the final average cluster radius is ∼13 nm (Figure 7). This corroborates the distribution of agglomerate sizes presented earlier as majority of the clusters were in the 0-28 nm diameter range. For the PMMA SiO<sub>2</sub> O samples, we observe a very narrow distribution of nanoparticle clusters sizes for all processing conditions. Even at low screw speed (100 rpm) well-dispersed systems are observed. With increased time spent in the extruder at higher energy input, a minor deterioration of the dispersion state is observed at  $100 \,\mathrm{rpm}$  ( $I_{\mathrm{filler}}$  decreases with time spent in the extruder and average cluster radius increases). This suggests prolonged time spent in the extruder can lead to re-agglomeration.

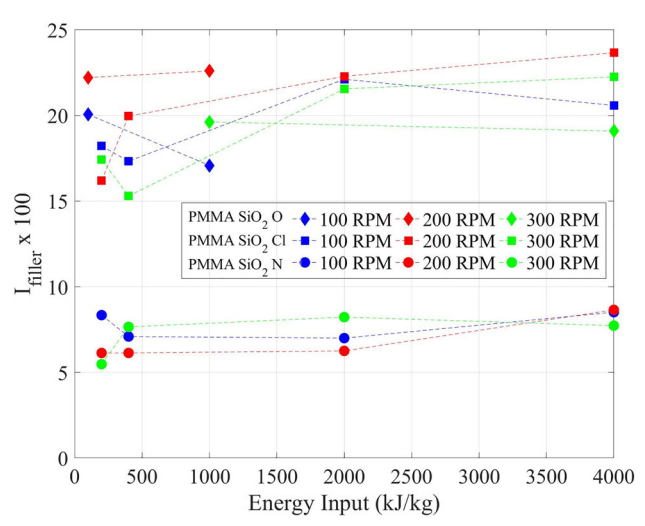


Figure 6. Ifiller vs processing energy for PMMA samples. All samples have a 2 wt% filler loading.

The results from the analysis of the PMMA systems can be summarized as follows:

- The higher the enthalpic compatibility between the polymer matrix and the nanoparticle surface, the more quickly the agglomerates break up (the more likely rupture is to occur) and good dispersion is achieved. If the fillers are too incompatible, good dispersion is never achieved.
- Amino-modified silica systems show a broad distribution of nanoparticle agglomerates. The dispersion state can be qualitatively described as having many large agglomerates along with smaller clusters. The quantified microstructural descriptors also indicate that the dispersion state is poor and improvement of the dispersion state is slow with increased screw speed and increased mixing energy input which is suggestive of primarily an erosion based process.
- Chloro-modified silica systems show a narrower distribution of nanoparticle agglomerates as compared to the amino-modified system. The dispersion state is significantly better and also shows further improvement with higher screw speed and mixing energy input. Thus with increase screw speed, rupture becomes more prominent.
- Octyl-modified silica systems show a very narrow distribution of clusters and a very uniform dispersion even at low screw speeds and low energy input. However, with prolonged processing of the material at the lower screw speed, the average cluster size was observed to increase and the dispersion deteriorated. This indicates that rupture dominates initially.

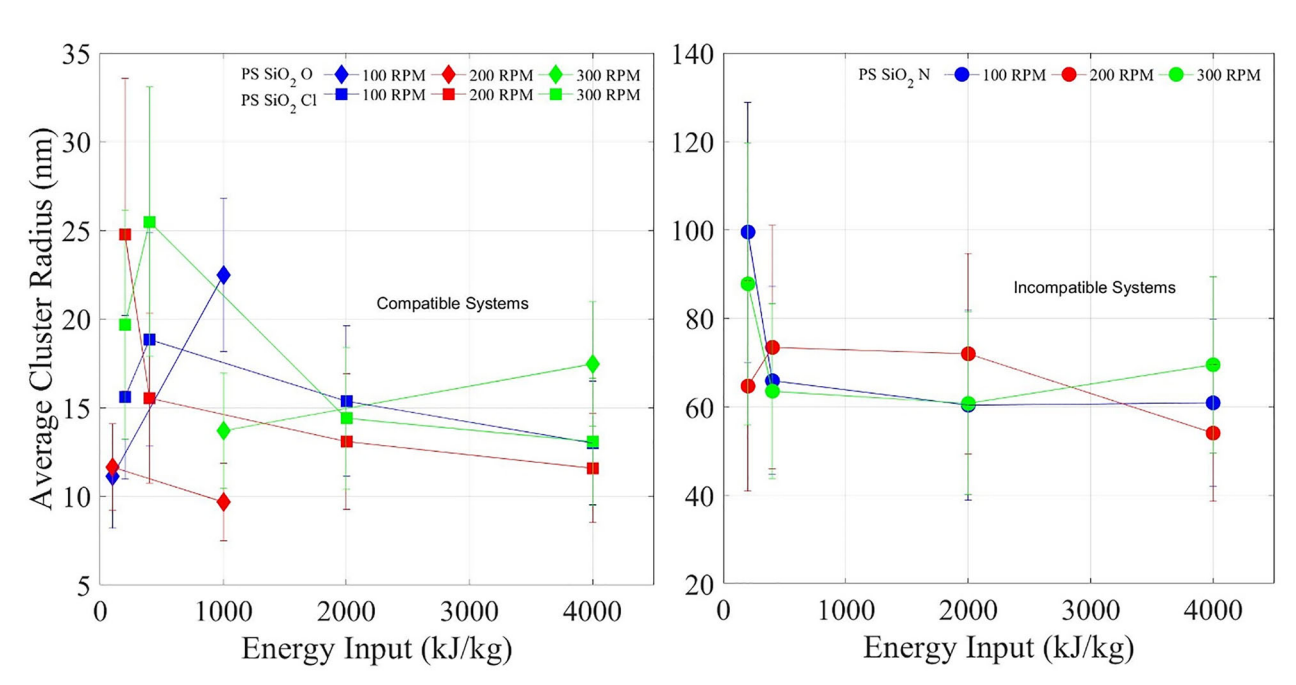


Figure 7. Average cluster radius vs processing energy input for PMMA samples. Filler loading of all samples is 2 wt%.

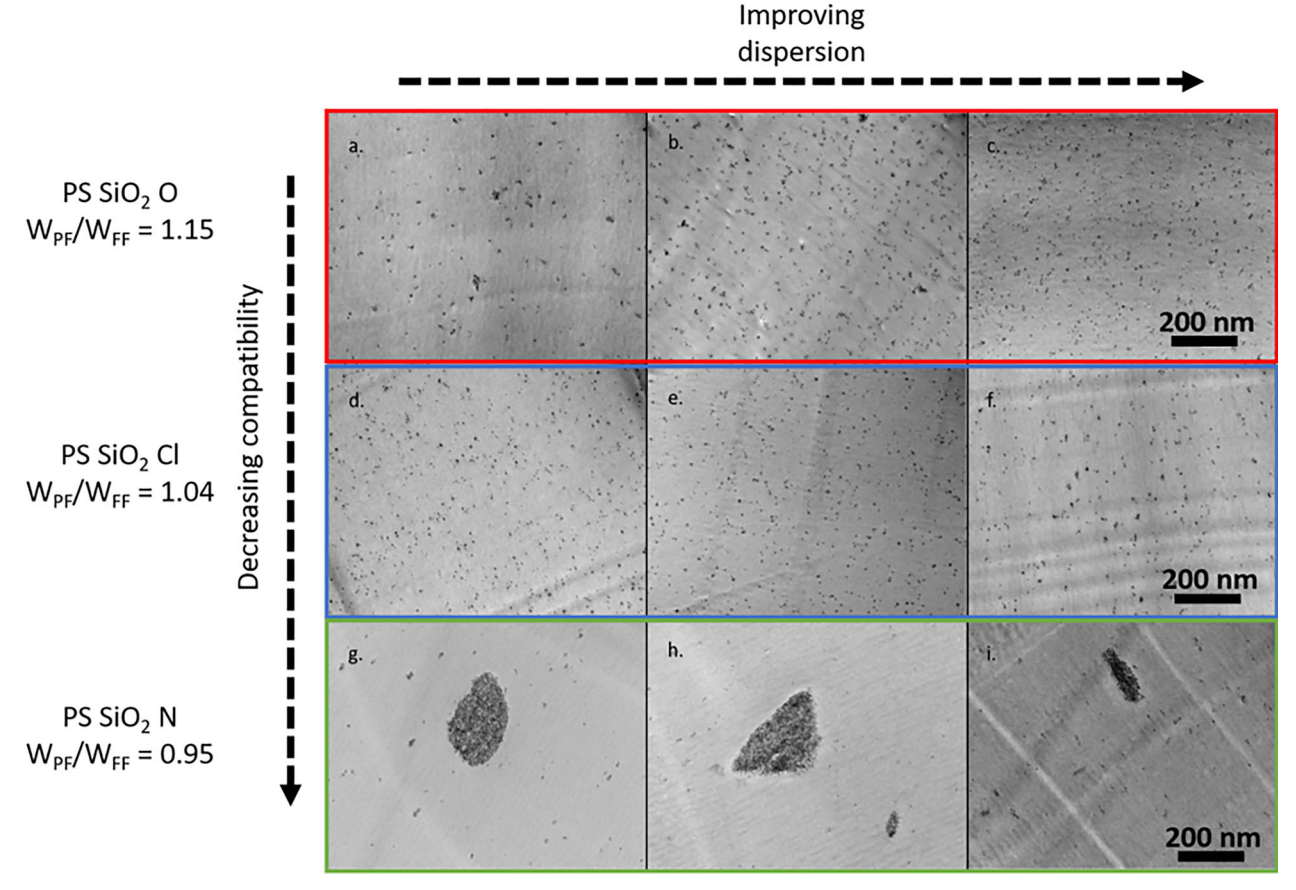


Figure 8. TEM images showing dispersions state for different PS-nanocomposite systems at 2 wt% filler loading: (a–c) PS SiO<sub>2</sub> O; (d–f) PS SiO<sub>2</sub> Cl; (g–i) PS SiO<sub>2</sub> N. All scale bars are 200 nm.

# PS nanocomposites post extrusion microstructure characterization

Figure 8 shows TEM images of PS based nanocomposites with silane modified silica nanoparticles. Similar to the microstructure of the PMMA systems, it is observed that the amino modified silica is not very well-dispersed in PS. This is to be expected as the surface chemistry is incompatible with PS. The agglomerates are large and few small nanoparticle clusters are visible. The SiO<sub>2</sub>–Cl and SiO<sub>2</sub>–O systems, which are compatible surface modifications with PS, are much better dispersed in comparison, with an even distribution of nanoparticle cluster. However, qualitatively, it is difficult to tell the difference between the dispersion quality of these two systems.

Histogram charts for systems processed at 200 rpm screw speed and 4000 kJ/kg energy input are shown in Figure 9a. The nanoparticle size distribution is narrower than all the PMMA system counterparts. This is possibly due to the lower temperature of processing of the PS compared to the PMMA (despite similar glass transition temperature), which leads to higher hydrodynamic stress. The PS SiO<sub>2</sub>–N (less compatible) system has a relatively large distribution of nanoparticles. Additionally, there is a steady decline in the number

of large nanoparticle clusters. In comparison, there are very few clusters larger than 42 nm for both the compatible systems (PS  $SiO_2$ –Cl and PS  $SiO_2$ –O). The distribution for the incompatible system is indicative of an erosion process and the compatible system is indicative of a rupture dominant process of deagglomeration, similar to the PMMA systems.

Figure 9b-d shows the evolution of the microstructure at 200 rpm screw speed for the octyl, chloro and amino modified silica-PS systems respectively. The PS SiO<sub>2</sub>-O samples have a narrow distribution of nanoparticle clusters. Increasing the energy input from 1000 to 4000 kJ/kg marginally increases the fraction of small clusters from 85% to 93%. In comparison, the PS SiO<sub>2</sub>-Cl also has a narrow distribution of cluster sizes, but the low energy sample has  $\sim$ 75% of clusters in the 0–28 nm range. However, with increasing the energy input, the fraction of small clusters reaches comparable values of 97%. The narrow distribution and fast deagglomeration is indicative of a rupture dominant process. The PS SiO<sub>2</sub>-N samples show a significant tail in the nanoparticle cluster distribution for the low energy input. With higher mixing energy, there is a reduction in the larger clusters, but they are observed to persist. For the highest energy input,  $\sim$ 16% of clusters are present outside of the 0–28 nm range. The distribution is narrower than the PMMA

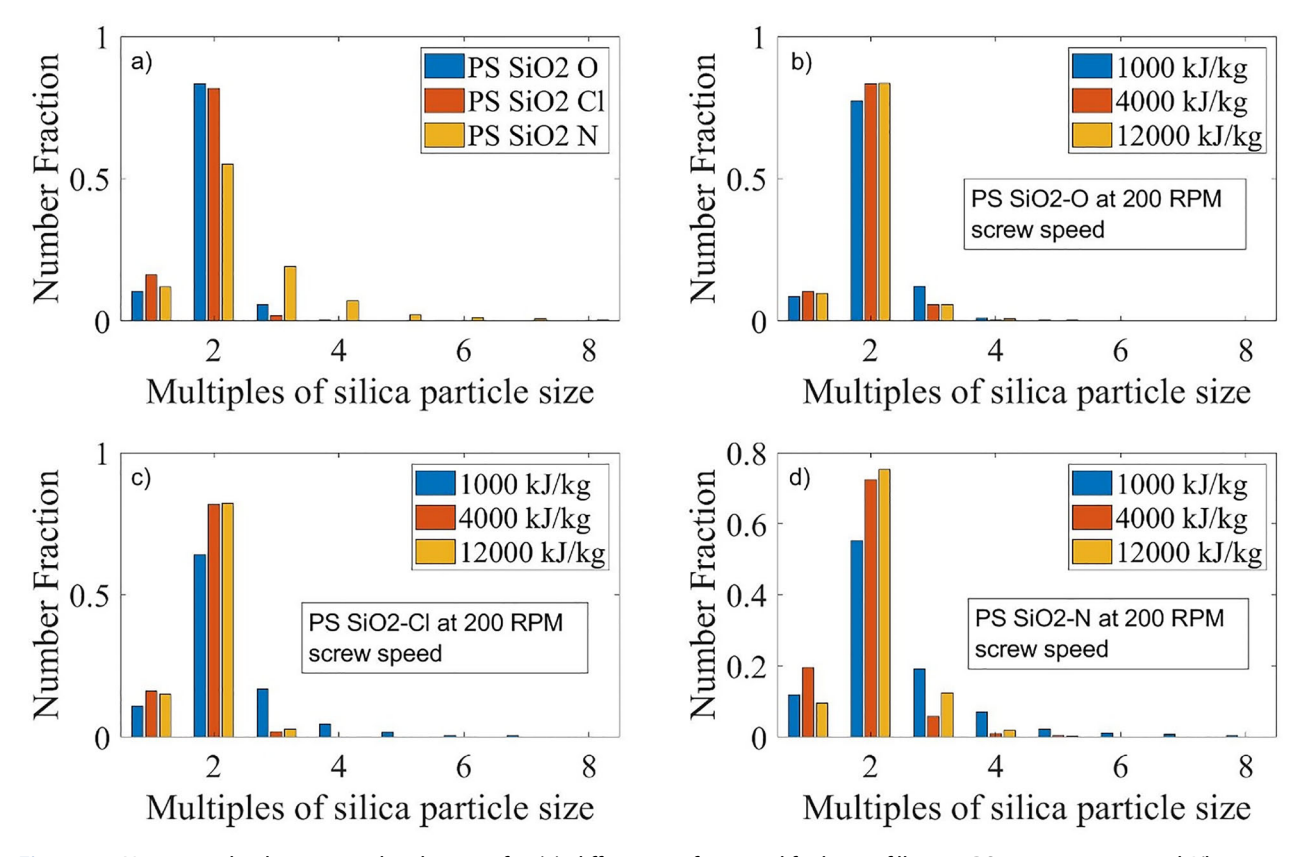


Figure 9. Nanoparticle cluster size distributions for (a) different surface modified nanofillers in PS at 200 rpm, 4000 kJ/kg processing energy; (b) PS SiO<sub>2</sub>–O at 200 rpm screw speed; (c) PS SiO<sub>2</sub>–Cl at 200 rpm screw speed; (d) PS SiO<sub>2</sub>–N at 200 rpm screw speed. All samples are at 2 wt% filler loading.

SiO<sub>2</sub>-N systems, but less uniform than the other PS systems.

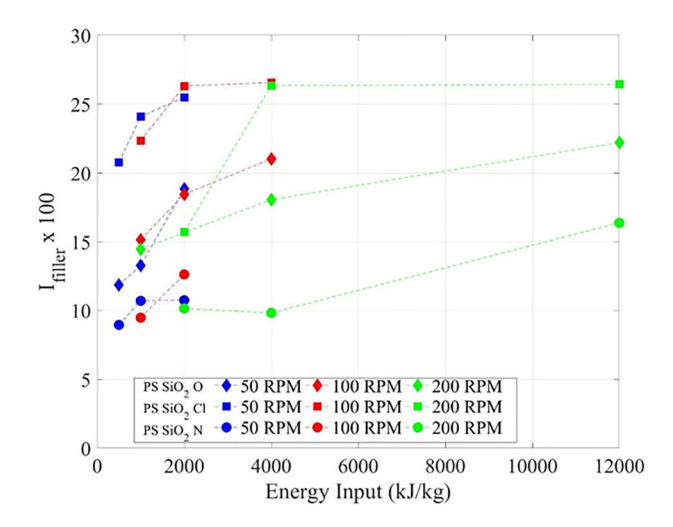
Figure 10a shows the  $I_{\text{filler}}$  vs energy input plots for the various PS samples and Figure 10b shows the evolution of the average cluster radius with time. For the incompatible amino system, the  $I_{\rm filler}$ values are similar to the amino-modified PMMA systems. However, much higher values of Ifiller are achieved with the very high energy input of 12,000 kJ/kg. Looking at the time spent in the extruder, at low screw speed of 50 rpm, the  $I_{\text{filler}}$ increases more slowly than at screw speeds of 100 and 200 rpm, suggesting that there is a transition from erosion to more rupture dominant response. This is supported by the fast average cluster size reduction at the high screw speeds shown in Figure 10b. At the lower screw speed, the cluster size levels to  $\sim$ 40 nm. PS SiO<sub>2</sub> Cl samples show a fast, efficient increase in  $I_{\text{filler}}$  at all screw speeds. The samples reach a maximum  $I_{\text{filler}}$  value of  $\sim$ 26 at low and high processing speeds. Combining the histogram data (Figure 10), I<sub>filler</sub> (Figure 10a) and average cluster radius trends (Figure 10b), we can say that the process for the compatible chloro modified system is rupture dominant.

All PS SiO2-O samples show a high degree of dispersion with large values of  $I_{\text{filler}}$  and small values of the average cluster radius. Similar to PS SiO<sub>2</sub>-Cl, we observe that at higher screw speeds, a greater

value of  $I_{\text{filler}}$  is achieved. Additionally, the average radius of nanoparticle clusters is smaller for the higher screw speed processing. Based on the observations of the cluster size distributions and the efficient dispersion process, we can conclude that the dominant mechanism for the compatible PS SiO2-O system is rupture.

The results from the analysis of the PS systems can be summarized as follows:

- Similar to the PMMA systems, nanoparticles with surface modifications compatible to the PS matrix achieved good dispersion, characterized by a high interfacial area, narrow cluster size distribution and low cluster Agglomerates of incompatible fillers could not be effectively broken down even with high screw speeds and long extrusion times, leading to poor dispersion.
- The maximum shear force generated during mixing for PS systems at low screw speeds was less than the cohesive strength between the nanoparticles, even for compatible systems. At higher screw speeds, the ratio of shear force to cohesive strength was found to be greater than 1 for compatible systems, and these exhibited efficient deagglomeration. The incompatible system, good dispersion was never achieved.



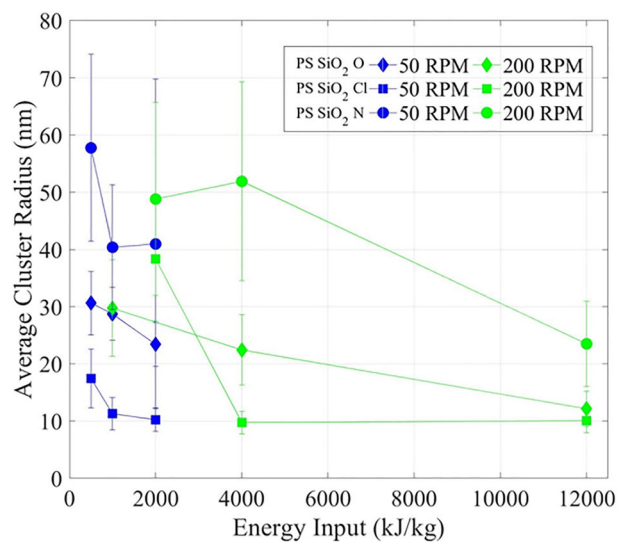


**Figure 10.** (a)  $I_{\text{filler}}$  vs processing energy for PS samples. All samples have a 2 wt% filler loading. (b) Average cluster radius vs processing time for PS samples. Filler loading of all samples is 2 wt%.

# **Discussion**

# Effect of wetting behavior on dispersion of nanoparticles

The cohesive strength,  $\sigma$ , of an agglomerate is given by the Rumpf equation [19]:

$$\sigma = \frac{(1 - \epsilon)}{\epsilon} \frac{F}{a^2} \tag{2}$$

where  $\epsilon$  is the porosity of the agglomerate, F is the adhesive force and a is the particle diameter.

Van der Waals forces make up the adhesive force between the particles in the cluster and can be calculated as follows [20]:

$$F = \frac{-H}{6D^2} \left( \frac{R_1 R_2}{R_1 + R_2} \right) \tag{3}$$

where H is the Hamaker constant, D is the interparticle distance and  $R_1$  and  $R_2$  are the radii of the two particles. For the system under study, the average diameter of nanoparticles is 14 nm. Interparticle

distance of 0.165 nm has been reported in the literature [21,22].

The wetting and incorporation of the polymer into the agglomerate changes the effective Hamaker constant and hence alters the adhesive force between the nanoparticles. The effective Hamaker constants for nanoparticles before and after incorporation of polymer are calculated using the following equation [23], and presented in Table 2:

$$A_{121} = \left(\sqrt{A_{11}} - \sqrt{A_{22}}\right)^2 \tag{4}$$

where  $A_{11}$  and  $A_{22}$  are the Hamaker constants of the particles and media, respectively, and  $A_{121}$  is the effective Hamaker constant.

The hydrodynamic shear stress on the spherical nanoparticle agglomerates is given by the following equation [24]:

$$\sigma_h = 2.5 \, \eta \, \dot{\gamma} \tag{5}$$

where  $\dot{\gamma}$  is the shear rate and  $\eta$  is the viscosity of the polymer nanocomposite melt. The maximum shear developed in a co-rotation twin screw extruder can be estimated from the following equation [21,25]:

$$\dot{\gamma} = \frac{\pi \cdot (D - 2\delta) \cdot N}{\delta} \tag{6}$$

where  $\dot{\gamma}$  is the shear rate, D is the screw diameter,  $\delta$  is the screw clearance with the barrel, and N is mixing speed. Viscosity of the nanocomposite systems was determined in the twin screw extruder by measuring the pressure drop across the length of the backflow channel at different screw speeds [26,27]. The data was fit to a power law model for shear thinning melts [28], to determine the viscosity at the higher shear rates present in the barrel of the extruder:

$$\eta = m\dot{\gamma}^{n-1} \tag{7}$$

where m is the consistency index and n is a measure of the non-Newtonian behavior of the melt.

Based on the above calculations, the maximum hydrodynamic shear for the two systems at different screws speeds is given in Table 3.

The incorporation of the polymer between the silica particles greatly reduces the Hamaker constant between the silica nanoparticles. However, the reduction depends on the quality of wetting and incorporation which is determined by the ratio of work of adhesions. For octyl-silica modified nanoparticles, the compatibility between the polymer melt and the nanoparticles is good and hence, the polymer melt is easily incorporated between the nanoparticles, reducing the adhesive force. This leads to a fast and effective deagglomeration process. For the amino-silane modified

Table 2. Calculated Hamaker constants and agglomerate cohesive strengths.

	Effective Hamaker Constant ( $\times$ 10 <sup>-20</sup> J)	Cohesive strength (kPa)
Silica	6.19	1.13 × 10 <sup>4</sup>
Silica-PMMA	$1.79 \times 10^{-2}$	86
Silica-PS	$1.56 \times 10^{-1}$	675

Table 3. Hydrodynamic shear stress developed in the extruder for the PMMA and PS systems.

	Maximum hydrodynamic shear stress (kPa)		
Extruder screw speed (rpm)	PMMA systems	PS systems	
300	523	809	
200	476	731	
100	406	615	
50	346	518	

nanoparticles, the compatibility is poor and hence, the polymer melt does not effectively wet the agglomerate. The removal of nanoparticle clusters is slow and from the surface of the agglomerate, leading to a broad distribution of cluster sizes. Boyle et al. [29] had observed similar results for fumed silica in PDMS and characterized the agglomerate failure mechanism into two categories- cohesive failure and adhesive failure. The former occurs when the fluid infiltration is minimal while the latter occurs when there is effective infiltration leading to lowering of the cohesive strength of the agglomerate.

Figure 11 (with data from this study and from the literature) shows a plot of the ratio of shear stress (calculated by Equation (6)) developed through mixing to the cohesive stress (calculated by eqn. 2) of the agglomerate vs. the ratio of work of adhesions of the polymer-filler to filler-filler. The left side of the plot shows incompatible systems which have a ratio of work of adhesions less than one. For such systems, the cohesive strengths of the agglomerates are high and infiltration of the agglomerate by the polymer is difficult. The right side of the plot shows compatible systems. These systems benefit from the infiltration of the nanoparticle agglomerate by the polymer. The upper and lower halves of the plot are demarcated as rupture and erosion dominant deagglomeration regions respectively. As rupture and erosion are processes that take place simultaneously [25], the regions are only marked by the dominant mechanism. When the shear stress  $\sim$  cohesive strength of the agglomerate, both rupture and erosion occur simultaneously and neither mechanism is dominant. On moving away from the center of the plot, shear stress > cohesive strength, rupture provides for a greater part of the deagglomeration, while for cases where the shear stress < cohesive strength, erosion is the dominant mechanism.

The data in Figure 11 represent a range of nanoparticle-polymer compatibilities and processing conditions. The PMMA systems from this study, represented by the (\*) marker, are shown as three sets of data points dependent on the surface modification of the nanoparticle surface. The PMMA SiO<sub>2</sub>-Cl and PMMA SiO<sub>2</sub>-O systems are present in the compatible-rupture dominant region of the map and the PMMA SiO<sub>2</sub>-N is present in the incompatible-erosion dominant region of the map. The multiple data points at the same  $W_{PF}/W_{FF}$  for a specific system represent the processing condition at different screw speeds. The PS systems have also been mapped on the plot and are represented by the ( ) marker. The compatible PS systems (chloro and octyl silane modified silica) experience shear stress values similar to the cohesive strength of the infiltrated agglomerate. At higher screw speeds, the processing is in the rupture dominant regime and at the lowest screw speed, the processing is in the erosion dominant regime. However, as these processing conditions are close to the boundary, both rupture and erosion are significantly active during the deagglomeration. Consequently, we see good dispersion for these samples. The incompatible PS system is in the erosion dominant regime for all processing speeds and the microstructure for these systems is characterized by large agglomerate, wide agglomerate size distributions and low values of  $I_{\text{filler}}$ .

Two systems from the literature have also been added to the plot. He et al. [24] worked on the dispersion of graphene nanoplatelets in a polypropylene matrix and used different screw configurations to develop variable levels of shear in the melt. The graphene-polypropylene system is plotted in Figure 11 by the (♦) marker. The system is highly incompatible ( $W_{PF}/W_{FF} = 0.61$ ). Additionally, processing conditions for the high shear screw configuration and low shear screw configuration are plotted. Cohesive strength values for large, medium sized and small agglomerates and shear values for the screw configurations were taken from the study. He et al. presented that based on agglomerate size distributions and shear values calculated for the different configuration, the high shear configuration lead to greater rupture of the nanoplatelet agglomerates and reduced the number of large agglomerates. Additionally, the low shear configuration had a broad range of nanoparticle agglomerate sizes. As the system had incompatible surface energetics, the final dispersion state for all systems still had micron sized agglomerates.

In comparison, Kasaliwal et al. [25] (plotted using the ( ) marker in Figure 11) worked on the processing of carbon nanotube-polycarbonate nanocomposites in a twin screw extruder at different screw



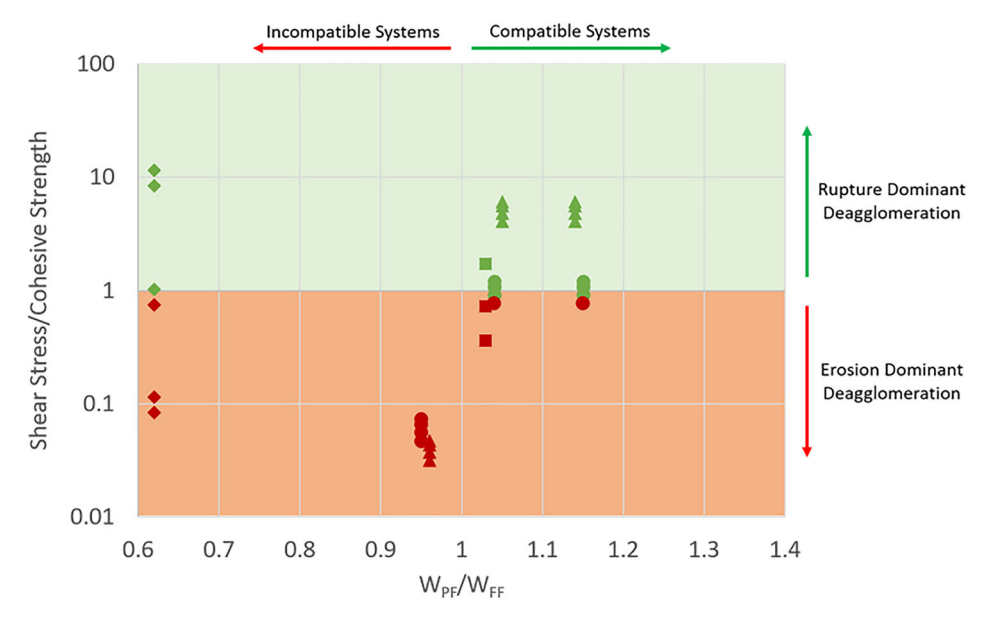


Figure 11. Map of deagglomeration regimes based on ratio of shear stress to cohesive stress and ratio of work of adhesion of the polymer-filler and filler-filler. (A) represents PMMA systems and ( ) represents PS systems from this study. (II) represents CNT-polycarbonate systems from [29] and ( ) represent graphene platelets-polypropylene systems from [28].

speeds. The system was compatible with a  $W_{\rm PF}/W_{\rm FF}$ ratio of 1.03. Based on the calculations made, the shear stress exceeded the cohesive strength of the agglomerates for the condition of high screw speed (300 rpm) but was less at the medium and low screw speeds (200 and 100 rpm, respectively). Hence, one condition is present in the rupture dominant regime and the latter two are in the erosion dominant regime. This suggests that the high screw speed condition led to deagglomeration due to rupture while the slow screw speed condition was an equal share of rupture and erosion. It is also interesting to note that the agglomerate size distributions in the rupture regime from the Kasaliwal study were narrower than the He study. This was observed in spite of the shear stress to cohesive strength ratio being greater for the latter system. This shows that infiltration of the polymer into the agglomerate is crucial for efficient deagglomeration and dispersion of the nanoparticles.

### **Conclusions**

Nanocomposites of surface modified silica nanoparticles in PMMA and PS matrices were prepared using a twin screw extruder with different processing parameters. The silane surface modification of the silica resulted in a range of compatibilities between the nanoparticle and the matrix polymer, characterized by the  $W_{PF}/W_{FF}$  ratio. TEM imaging along with image analysis was done to determine quantified descriptors of nanoparticle dispersion.

It was found that nanoparticle-polymer compatibility was the most important characteristic in determining the dispersion state and the dominant deagglomeration process. For incompatible systems,

the breakdown of nanoparticle clusters was slow and the distribution of cluster sizes revealed a mix of large clusters and small clusters, indicating an erosion dominant process. For compatible systems, the process of nanoparticle cluster size reduction was found to be very fast and efficient. High values of  $I_{\text{filler}}$  were achieved and the distribution of nanoparticle clusters was narrow. Hence, the surface energetics between the nanoparticle and polymer were leading to a transition from erosion to rupture.

The role of the incorporation of the polymer matrix in the agglomerate was quantitatively assessed and was found to greatly reduce the cohesive strength between the nanoparticles. For PMMA systems, the resultant cohesive strength was less than the shear produced in the polymer by the extruder. Hence, for the compatible surface modifications, the favorable wetting of the agglomerate led to a rupture dominant process of agglomerate breakdown. For the incompatible surface modification (amino-silane), the cohesive strength of the agglomerate exceeded the shear developed in the extruder and the agglomerate breakdown was slow. Increasing the shear in the extruder by increasing the screw speed did speed up the deagglomeration process, but the average cluster sizes and amount of interfacial filler remained large and small respectively. For the PS nanocomposites, the incorporation of the polymer into the agglomerate greatly reduced the force between the nanoparticles. However, in the PS system, the shear produced in the extruder exceeded the cohesive strength of the agglomerate only at high screw speeds. At the lower screw speed (50 rpm), the shear stress was considerably lower. This resulted in comparatively slower



deagglomeration even when the compatibility between the modified nanoparticle was favorable.

The analysis was also applied to two studies in the literature and found to be in good agreement with the results presented. The highly incompatible system of graphene nanoplatelets in polypropylene exhibited a dispersions state with micron sized agglomerates, even when the shear stress from the extruder exceeded the cohesive strength of the agglomerates. In contrast, the compatible system of carbon nanotubes in a polycarbonate matrix exhibited better dispersion and deagglomeration took place by a rupture dominant mechanism at the higher processed screw speed.

#### **Disclosure statement**

The authors would like to declare no conflicts of interest.

## **Funding**

This work was supported by the National Science Foundation under Grant no. CMMI - 1333977 (Rennselaer Polytechnic Institute), CMMI - 1729452 (Rennselaer Polytechnic Institute), and CMMI 1729743 (Northwestern University).

# **Notes on contributors**

Aditya Shanker Prasad received his B. Tech. in Ceramic Engineering from the Indian Institute of Technology (BHU), India and his Ph.D. from Rensselaer Polytechnic Institute. His research focused on building structureproperty-processing relationships for polymer nanodielectrics.

Yixing Wang received his BS in Engineering Mechanics from Harbin Institute of Technology and his Ph.D. from Department of Mechanical Engineering Northwestern University. His doctoral research focused on finite element modeling of dielectric properties in polymer nanocomposite.

Xiaolin Li received his BS in Engineering Mechanics from Shanghai Jiao Tong University, China. He completed his Ph.D. from the Theoretical and Applied Mechanics program at Northwestern University, where he worked on data-driven materials design for polymer nanocomposites.

Akshay Iyer is a graduate student at the Department of Mechanical Engineering at Northwestern University. His research focuses on developing computational methods for data driven design of material systems.

Wei Chen is the Wilson-Cook Professor in Engineering Design and professor of mechanical engineering at Northwestern University. Her research focuses on stochastic multiscale analysis and materials design, design of metamaterials and data science in design and advanced manufacturing.

L. Catherine Brinson is Sharon C. and Harold L. Yoh, III Distinguished Professor and Chair of the Department of Mechanical Engineering and Materials Science at Duke University. Her work focuses on characterizing and modeling advanced materials systems at scales spanning the range of molecular interactions, micromechanical and macroscopic behavior.

Linda S. Schadler is the Dean of Engineering and Mathematical Sciences at the University of Vermont and professor in the Mechanical Engineering Department. Her research focuses on the dielectric, mechanical, and optical properties of polymer nanocomposites.

#### **ORCID**

Aditya Shanker Prasad (D) http://orcid.org/0000-0001-6967-6824

#### References

- Arjmand M, Sundararaj U. Broadband dielectric properties of multiwalled carbon nanotube/polystyrene composites. Polym Eng Sci. 2015;55(1):173-179.
- Bell M, Krentz T, Keith Nelson J, et al. Investigation of dielectric breakdown in silica-epoxy nanocomposites using designed interfaces. J Colloid Interface Sci. 2017;495:130-139.
- Li Y, Tao P, Viswanath A, et al. Bimodal surface ligand engineering: the key to tunable nanocomposites. Langmuir. 2013;29(4):1211-1220.
- Natarajan B, Li Y, Deng H, et al. Effect of interfacial energetics on dispersion and glass transition temperature in polymer nanocomposites. Macromolecules. 2013;46(7):2833-2841.
- Natarajan B, Neely T, Rungta A, et Thermomechanical properties of bimodal brush modified nanoparticle composites. Macromolecules. 2013;46(12):4909-4918.
- Edgecombe SR, Gardiner JM, Matsen MW. Suppressing autophobic dewetting by using a bimodal brush. Macromolecules. 2002;35(16): 6475-6477.
- Kim P, Jones SC, Hotchkiss PJ, et al. Phosphonic acid-modified barium titanate polymer nanocomposites with high permittivity and dielectric strength. Adv Mater. 2007;19(7):1001-1005.
- Bolen W, Colwell R. Intensive mixing. Soc Plast Eng J. 1958;14(8):24-28.
- Manas-Zloczower I, Nir A, Tadmor Z. Dispersive mixing in internal mixers - a theoretical-model based on agglomerate rupture. Rubber Chem Technol. 1982;55(5):1250-1285.
- Tadmor Z. Forces in dispersive mixing. Ind Eng Chem Fund. 1976;15(4):346-348.
- 11. Shiga S, Furuta M. Processability of electron-paramagnetic-res in an internal mixer. Morphological-changes of carbon-black agglomerates during mixing. Rubber Chem Technol. 1985; 58(1):1-22.
- Rwei SP, Manas-Zloczower I, Feke DL. Observation of carbon-black agglomerate dispersion in simple shear flows. Polym Eng Sci. 1990;30(12):701-706.
- 13. SP, Manas-Zloczower I, Feke DL. Characterization of agglomerate dispersion by

- erosion in simple shear flows. Polym Eng Sci. 1991; 31(8):558-562.
- 14. Rwei SP, Horwatt SW, Manas-Zloczower I, et al. Observation and analysis of carbon-black agglomerate dispersion in simple shear flows. Int Polym Proc. 1991;6(2):98-102.
- 15. Ke K, Wang Y, Liu X-Q, et al. A comparison of melt and solution mixing on the dispersion of carbon nanotubes in a poly(vinylidene fluoride) matrix. Compos B Eng. 2012;43(3):1425-1432.
- Kasaliwal G, Goldel A, Potschke P. Influence of processing conditions in small-scale melt mixing and compression molding on the resistivity and morphology of polycarbonate-MWNT composites. J Appl Polym Sci. 2009;112(6):3494-3509.
- Villmow T, Potschke P, Pegel S, et al. Influence of twin-screw extrusion conditions on the dispersion of multi-walled carbon nanotubes in a poly(lactic acid) matrix. Polymer. 2008;49(16):3500-3509.
- Hassinger I, Li X, Zhao H, et al. Toward the development of a quantitative tool for predicting dispersion of nanocomposites under non-equilibrium processing conditions. J Mater Sci. 2016;51(9):
- Rumpf H. Theory of tensile strength of agglomerates in which transfer of force takes place at points of contact of particles. Chem Ing Tech. 1970;42(8):
- Hamaker H. The London-van der Waals attraction between spherical particles. Physica. 1937;4(10): 1058-1072.
- Tanahashi M, Hirose M, Lee JC, et al. Organic/ inorganic nanocomposites prepared by mechanical smashing of agglomerated silica ultrafine particles in molten thermoplastic resin. Polym Adv Technol. 2006;17(11-12):981-990.

- Israelachvili JN. Van der Waals dispersion force contribution to works of adhesion and contact angles on basis of macroscopic theory. J Chem Soc, Faraday Trans 2. 1973;69(12):1729-1738.
- 23. Borse NK, Kamal MR. Estimation of stresses required for exfoliation of clay particles in polymer nanocomposites. Polym Eng Sci. 2009;49(4): 641-650.
- He SH, Zhang JJ, Xiao XT, et al. Study on the morphology development and dispersion mechanism of polypropylene/graphene nanoplatelets composites for different shear field. Compos Sci Technol. 2017;153:209-221.
- Kasaliwal GR, Pegel S, Goldel A, et al. Analysis of agglomerate dispersion mechanisms of multiwalled carbon nanotubes during melt mixing in polycarbonate. Polymer. 2010;51(12):2708-2720.
- Leroy E, Jacquet P, Coativy G, 26. Compatibilization of starch-zein melt processed blends by an ionic liquid used as plasticizer. Carbohydr Polym. 2012;89(3):955-963.
- Yousfi M, Alix S, Lebeau M, et al. Evaluation of rheological properties of non-Newtonian fluids in micro rheology compounder: experimental procedures for a reliable polymer melt viscosity measurement. Polym Test. 2014;40:207-217.
- Mallette JG, Soberanis RR. Evaluation of rheological properties of non-Newtonian fluids in internal mixers: An alternative method based on the power law model. Polym Eng Sci. 1998;38(9):1436-1442.
- 29. Manas-Zloczower I, JF, Feke Hydrodynamic analysis of the mechanisms of agglomerate dispersion. Powder Technol. 2005; 153(2):127-133.